Nonlinear Dyn (2011) 64: 237–252
DOI 10.1007/s11071-010-9858-4

ORIGINAL PAPER

Effects of flexible support stiffness on the nonlinear dynamic characteristics and stability of a turbopump rotor system

Changqing Bai · Qingyu Xu · Jiyan Wang

Received: 4 February 2010 / Accepted: 28 September 2010 / Published online: 19 October 2010

Abstract Using a flexible support is an efficient approach to solving the subsynchronous problems in a turbopump. In this paper, nonlinear rotordynamic analysis of a liquid fuel turbopump with a flexible support is presented using a dynamic modeling including two key destabilizing factors, nonlinear hydrodynamic forces induced by seals and internal rotor damping. The methodology of the partitioned direct integration method (PDIM) is described for reducing the computational efforts efficiently. Combining the PDIM and the shooting method, a nonlinear stability analysis of the rotor system is performed effectively. The numerical results, which are in good agreement with test data, indicate that the effects of flexible support stiffness k on the dynamic characteristics and stability of the rotor system are significant. The first critical speed of the rotor system rises as a nonlinear function of k markedly. The second critical speed varies slightly and approximates a linear variation as k increases. The onset speed of instability of the rotor system rises initially and then reduces as k increases. The effect of seal nonlinearities at low k is contrary to that at high k and the effect of seal length on the system stability is more significant than that of seal radius. The results explain the nature of the subsynchronous motion of a turbopump rotor system with flexible support and can be used in the design and operation of a liquid fuel turbopump rotor system to eliminate its rotordynamic problem.

Keywords Turbopump · Flexible support · Seal · Internal damping · Nonlinear stability · Rotordynamic

C. Bai (✉) · Q. Xu
School of Aerospace, Xi'an Jiaotong University, Xi'an 710049, China
e-mail: baichq@mail.xjtu.edu.cn

J. Wang
School of Science, China University of Mining and Technology, Xuzhou 221008, China

1 Introduction

A liquid rocket engine is widely employed in a space launch vehicle with a high thrust-to-weight ratio. A turbopump, described as the heart of the liquid rocket engine, is used to supply high-pressure cryogenic fuel, such as liquid hydrogen or liquid oxygen, to a liquid rocket engine. The operating rotational speed of a turbopump, especially a liquid hydrogen turbopump, is usually very high to increase the operating efficiency and reduce the turbopump weight.

The liquid hydrogen turbopump, as a key role in the liquid rocket engine, has presented various rotordynamic problems because of the extremely high operating speed and extraordinarily low viscosity of liquid hydrogen. The SSME (Space Shuttle Main Engine) HPFTP (High Pressure Fuel Turbopump) designed in the 1970s has been subject to a rotordynamic instability problem, characterized by large and

damaging subsynchronous whirling motion. Hydrodynamic forces due to seals had a significant destabilizing effect on the turbopump, and its stability can be improved with appropriate interstage seal designs, as described in Ref. [1, 2]. Childs's analysis in Ref. [3] revealed that the interstage seals of an ATD (Alternate Technology Development) HPFTP represented a major source of destabilizing forces. Severe subsynchronous problems have also been encountered in the liquid hydrogen turbopump of the Chinese CZ-3 rocket (see Ying [4]) and the Japanese LE-7 turbopump (see Okayasu et al. [5]). The tests demonstrated that the significant source of subsynchronous vibrations was the internal rotor damping. This problem was remedied by supporting the turbine end bearing on a flexible support [6]. As mentioned above, it can be found that seals and internal damping are two key destabilizing factors and using a flexible support is an efficient approach to solve the rotordynamic problems in a liquid hydrogen turbopump. Hence, considering the effects of seals and internal damping, to investigate the rotordynamic characteristics and stability of the liquid hydrogen turbopump with flexible support is mandatory and significant to improve its stability performance and eliminate its subsynchronous problem in design.

Childs [2], Chen [6], and Zhang [7] employed Black's results in Ref. [8] to analyze the effect of hydrodynamic forces due to seals on the stability of a liquid hydrogen turbopump. Black's results had been experimentally verified for axial Reynolds numbers out to approximately 20,000, but the HPFTP seals operate at axial Reynolds numbers on the order of 500,000. Further, the linear model and stability analysis in the above work cannot explain some aspects of the test data and analyze the nature of the subsynchronous motion. This problem can only be resolved by nonlinear modeling and the corresponding analysis. Describing the radial stiffness, damping, and inertia effects of fluid film inside the seals as nonlinear functions of the rotor eccentricity ratio, Muszynska [9, 10] proposed a nonlinear model of fluid dynamic forces due to seals, and the analysis results obtained from this model were validated with many experiment results. Using the Muszynska model, Ding et al. [11] and Li et al. [12] investigated the nonlinear behavior and stability of a Jeffcott rotor/seal system. Bai et al. [13] employed the Muszynska model to study the effect of seal hydrodynamic forces on the nonlinear dynamic stability of a turbopump rotor system, but did not consider the effects of internal rotor damping and flexible support.

The importance of including flexible supports in rotordynamic analysis was discussed by Nicholas et al. [14]. They predicted the critical speed of a steam turbine rotor with flexible support. Guo et al. [15] investigated the instability boundary for rotor-hydrodynamic bearing systems with external flexible damped bearing supports. It was shown that the characteristics of the flexible support had a strong effect on the system stability. Seong et al. [16] performed a critical speed analysis for a 30-ton thrust demonstrator turbopump considering the casing structural flexibility. It was found that the effect of the casing structural flexibility reduces the critical speeds of the turbopump. Qin et al. [17] studied the nonlinear response and bifurcation of a rotor with a squeezed film damper supported on an elastic foundation and found that the influence of support stiffness on system response was significant. Chang-Jian and Chen [18, 19] investigated the nonlinear dynamic response of a rotor-bearing system considering the quadratic damping and the dynamic responses of a flexible rotor supported by porous and nonporous bearings with nonlinear suspension. The numerical results could provide some useful insights into the design and development of rotor-bearing systems for rotating machinery. But the nonlinear rotordynamic analysis of a turbopump rotor system with flexible support is lacking, and little effort has been expended on both flexible support and destabilizing factors effects.

In this paper, the present study is intended to cast light on the nonlinear rotordynamic analysis of a liquid fuel turbopump with a flexible support with the aid of the finite element technique taking into account the effects of seals and internal damping. A Partitioned Direct Integration Method (PDIM) is advanced for reducing the computational efforts. The numerical results obtained from the nonlinear model are compared to the test results for validating the presented dynamic model. Combining with PDIM and the shooting method, the effects of flexible support on the nonlinear dynamic characteristics and stability of the turbopump rotor system is investigated efficiently.

2 Rotordynamics model

The liquid fuel turbopump, as shown in Fig. 1(a), combines a pump and a turbine on a single shaft which is

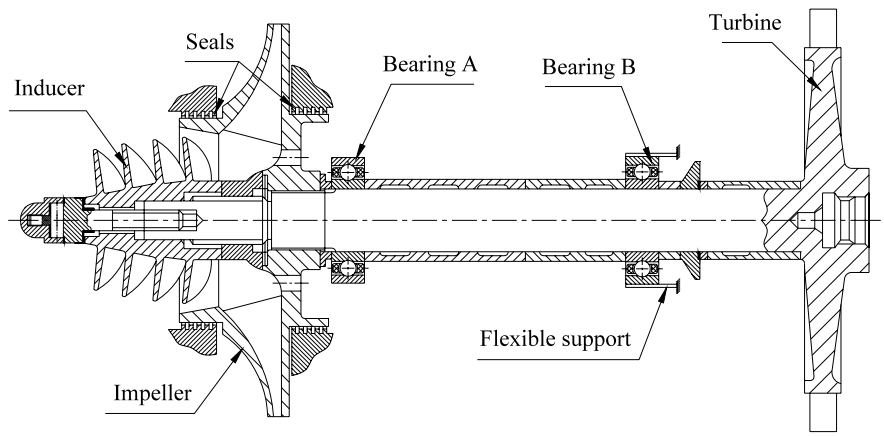

(a) A liquid fuel turbopump rotating assembly

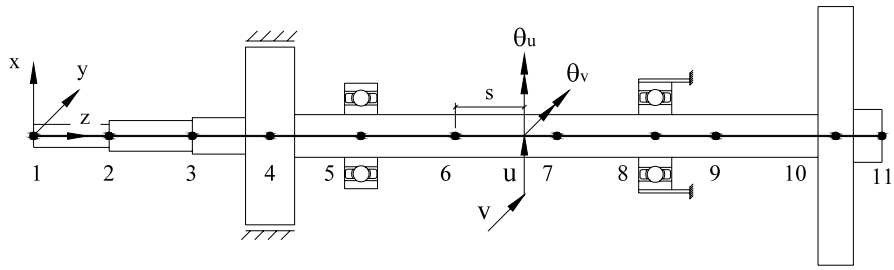

(b) Rotordynamic finite element model, 1 ~ 11: node number

Fig. 1 A liquid fuel turbopump and its rotordynamic finite element model

supported by two ball bearings, A and B. The liquid seals restrict leakage flow along the front side of the impeller from impeller discharge to impeller inlet, and the seal arrangements are represented in Fig. 1(a).

As shown in Fig. 1(b), the liquid fuel turbopump rotor system as illustrated in Fig. 1(a) was modeled as an assembly of 10 finite elements and 11 nodes using a finite element technique. The impeller and the turbine were concentrated on two disks located at nodes 4 and 10. The bearings A and B are located at nodes 5 and 8. The dynamic forces due to liquid seals arranged at the impeller discharge and inlet were equivalent to the concentrated forces applied on node 4.

Each rotor element is modeled as an eight-degree-of-freedom element with two translations and two rotations at each end. Figure 1(b) shows the displacements of a typical cross section, located at a distance s from the element end, denoted by u, v, θ_u and θ_v. Translations $\{u\ v\}^{\mathrm{T}}$ and rotations $\{\theta_u\ \theta_v\}^{\mathrm{T}}$ of a point in the element can be related to the node displacements $\{q^e(t)\}$ as

$$\{u \quad v\}^{\mathrm{T}} = \left[N_t(s)\right]\left\{q^e(t)\right\}, \tag{1}$$

$$\{\theta_u \quad \theta_v\}^{\mathrm{T}} = \left[N_r(s)\right]\left\{q^e(t)\right\}, \tag{2}$$

where $[N_t(s)]$ and $[N_r(s)]$ are the translational and rotational shape function matrices, respectively. The shape functions established by Nelson [20] for a Timoshenko beam element are utilized in this study. By introducing the above equations into the kinetic and potential energy expressions, carrying out the integrations over the element length, and applying the extended Hamilton's principle, the matrix equations of motion for the undamped element can be written in the form

$$\left[M^e\right]\left\{\ddot{q}^e\right\} - \omega\left[G^e\right]\left\{\dot{q}^e\right\} + \left[K^e\right]\left\{q^e\right\} = \left\{Q^e\right\}, \tag{3}$$

where ω is the rotational speed. $[M^e]$, $[G^e]$ and $[K^e]$ are the mass, gyroscopic, and stiffness matrices of an element, respectively. $\{Q^e\}$ is the vector of generalized forces of an element.

Internal damping can be divided into a viscous damping component and a hysteretic component. Viscous damping is induced in a rotating shaft due to its internal resistance to strain. The viscous damping forces along the u and v directions, F_{du} and F_{dv}, represented by Gunter [21] for a single mass rotor are

$$\begin{Bmatrix} F_{du} \\ F_{dv} \end{Bmatrix} = -\begin{bmatrix} \eta_v & 0 \\ 0 & \eta_v \end{bmatrix} \begin{Bmatrix} \dot{u} \\ \dot{v} \end{Bmatrix} - \begin{bmatrix} 0 & -\omega\eta_v \\ \omega\eta_v & 0 \end{bmatrix} \begin{Bmatrix} u \\ v \end{Bmatrix}, \tag{4}$$

where η_v is the coefficient of internal viscous damping.

Hysteretic damping is the other internal damping, induced due to a lag of the neutral stress plane from the geometrical one by an angle, γ_h. This effect couples the flexural bending moments along the u and v directions, M_{du} and M_{dv}, such that

$$\begin{Bmatrix} M_{dv} \\ M_{du} \end{Bmatrix} = EI \begin{bmatrix} \cos\gamma_h & \sin\gamma_h \\ -\sin\gamma_h & \cos\gamma_h \end{bmatrix} \begin{Bmatrix} \theta'_u \\ \theta'_v \end{Bmatrix}, \tag{5}$$

where γ_h is called the loss angle and is given by

$$\sin\gamma_h = \frac{\eta_h}{\sqrt{1+\eta_h^2}}. \tag{6}$$

Internal viscous damping and hysteretic damping can be properly incorporated into the finite element model employing the virtual work principle in [22]. The viscous damping forces and moments due to hysteretic damping, expressed in (4) and (5), can be introduced into the element equations through the virtual work expression

$$\{Q_d^e\} = \int_0^l [N_t(s)]^{\mathrm{T}} \begin{Bmatrix} F_{du} \\ F_{dv} \end{Bmatrix} \mathrm{d}s, \tag{7}$$

$$\delta W_d = \int_0^l \begin{Bmatrix} \delta\theta_u \\ \delta\theta_v \end{Bmatrix}^{\mathrm{T}} \begin{Bmatrix} M_{du} \\ M_{dv} \end{Bmatrix}' \mathrm{d}s. \tag{8}$$

Then considering the internal rotor damping, the element equations (see (3)) can be expressed as follows:

$$[M^e]\{\ddot{q}^e\} + \omega([D_v^e] - [G^e])\{\dot{q}^e\} + (\cos\gamma_k[K^e] + [D_d^e] + [D_h^e])\{q^e\} = \{Q^e\}, \tag{9}$$

where $[D_d^e]$ and $[D_v^e]$ are the internal viscous damping matrix of an element, with the factor of displacements and velocities, respectively. $[D_h^e]$ is the hysteretic damping matrix of an element. The individual matrices appearing in the above equations are presented in detail in Nelson [20] and Hashish et al. [22].

The flexible support model is described as eight spring and damping coefficients. The support reactions at the flexible support, F_{bu} and F_{bv}, are obtained from

$$\begin{Bmatrix} F_{bu} \\ F_{bv} \end{Bmatrix} = -\begin{bmatrix} c_{uu} & c_{uv} \\ c_{vu} & c_{vv} \end{bmatrix} \begin{Bmatrix} \dot{u}_b \\ \dot{v}_b \end{Bmatrix} - \begin{bmatrix} k_{uu} & k_{uv} \\ k_{vu} & k_{vv} \end{bmatrix} \begin{Bmatrix} u_b \\ v_b \end{Bmatrix}, \tag{10}$$

where u_b and v_b are the nodal displacements referring to the flexible support.

The nonlinear equations of motion of the complete liquid fuel turbopump rotor system, consisting of components (9) and (10), are of the form

$$[M]\{\ddot{q}\} + [C]\{\dot{q}\} + [K]\{q\} = \{F_u(t)\} + \{F_s(q,\dot{q})\}, \tag{11}$$

where $[M]$, $[C]$ and $[K]$ are the mass, damping, and stiffness matrices of the 44-degrees-of-freedom system obtained by assembling the element matrices and flexible support reactions. $\{q\}$ is the nodal displacement vector of the rotor system. $\{F_u\}$ and $\{F_s\}$ are the vectors of unbalanced forces and liquid dynamic forces due to the seal, respectively.

The Muszynska model [9, 10] can accurately represent the nonlinear liquid dynamic forces due to seals, and a key variable called the fluid average circumferential velocity ratio, τ, is assumed to describe the characteristic of the fluid motion as a whole. Although the compressibility of liquid fuel, such as liquid hydrogen, is neglected, the Muszynska model could be the most suitable model for the existing nonlinear model for the liquid fuel seal owing to its availability and convenience. It is better at explaining the nonlinear behavior and clarifying the nature of the subsynchronous motion caused by seals. The Muszynska model expresses a force-motion relationship of the form

$$\begin{Bmatrix} F_{su} \\ F_{sv} \end{Bmatrix} = -\begin{bmatrix} K_s - m_f\tau^2\omega & \tau\omega D_s \\ -\tau\omega D_s & K_s - m_f\tau^2\omega \end{bmatrix} \begin{Bmatrix} u_s \\ v_s \end{Bmatrix} - \begin{bmatrix} D_s & 2\tau m_f\omega \\ -2\tau m_f\omega & D_s \end{bmatrix} \begin{Bmatrix} \dot{u}_s \\ \dot{v}_s \end{Bmatrix} - \begin{bmatrix} m_f & 0 \\ 0 & m_f \end{bmatrix} \begin{Bmatrix} \ddot{u}_s \\ \ddot{v}_s \end{Bmatrix}, \tag{12}$$

where F_{su} and F_{sv} are seal forces along the u and v directions, respectively. u_s and v_s are the nodal displacements referred to the seal. K_s, D_s and m_f are the fluid film radial stiffness, damping, and inertia coefficients, respectively. K_s, D_s and τ, which are the nonlinear functions of the rotor eccentricity, were given by Muszynska et al. [10] as follows:

$$\left.\begin{array}{ll} K_s = K_0\left(1-e^2\right)^{-n} & \\ D_s = D_0\left(1-e^2\right)^{-n} & (n=0.5\sim 3), \\ \tau = \tau_0(1-e)^b & (0<b<1, \tau_0<0.5). \end{array}\right\} \tag{13}$$

In these equations, e is the relative eccentricity, $e = \sqrt{u_s^2+v_s^2}/c$, and c is the seal radial clearance. The coefficients K_0, D_0 and m_f may be calculated with Black–Childs equations in [23], which are represented in the Appendix.

3 Partitioned direct integration method for nonlinear rotordynamic analysis [24]

With respect to the system of equations (11), it can be noted that the nonlinear seal forces, as shown in (13), are only acting on node 4 as equivalent forces, which relate to nothing more than the motion state of node 4. Thus, the system of equations (11) can be partitioned into linear and nonlinear components and written as the following partition forms:

$$\begin{aligned} &\begin{bmatrix} [M_{11}] & [M_{12}] \\ [M_{21}] & [M_{22}] \end{bmatrix} \begin{Bmatrix} \{\ddot{q}_1\} \\ \{\ddot{q}_2\} \end{Bmatrix} + \begin{bmatrix} [C_{11}] & [C_{12}] \\ [C_{21}] & [C_{22}] \end{bmatrix} \begin{Bmatrix} \{\dot{q}_1\} \\ \{\dot{q}_2\} \end{Bmatrix} \\ &\quad + \begin{bmatrix} [K_{11}] & [K_{12}] \\ [K_{21}] & [K_{22}] \end{bmatrix} \begin{Bmatrix} \{q_1\} \\ \{q_2\} \end{Bmatrix} \\ &= \begin{Bmatrix} \{F_{u1}(t)\} \\ \{F_{u2}(t)\} \end{Bmatrix} + \begin{Bmatrix} \{0\} \\ \{F_{s2}(\{q_2\},\{\dot{q}_2\})\} \end{Bmatrix}, \end{aligned} \tag{14}$$

where $\{q_1\} \in R^{n_1}$ and $\{q_2\} \in R^{n_2}$ denote the displacement vectors referring to linear and nonlinear components of the system displacement vector $\{q\}$, respectively. $\{q_1\}$ and $\{q_2\}$ can be defined as linear and nonlinear coordinates, respectively. Note that the nonlinear coordinates concern no more than the displacements of node 4, $\{q_2\} = \{u_s \ v_s\}^{\mathrm{T}}$ and $\{F_{s2}\} = \{F_{su} \ F_{sv}\}^{\mathrm{T}}$. It is indicated that the number of nonlinear coordinates is much less than the number of linear coordinate, i.e. $n_2 \ll n_1$, which is also a feature of most complex nonlinear rotor systems. The expanded formulas of (14) can be expressed as

$$\begin{aligned} &[M_{11}]\{\ddot{q}_1\} + [C_{11}]\{\dot{q}_1\} + [K_{11}]\{q_1\} + [M_{12}]\{\ddot{q}_2\} \\ &\quad + [C_{12}]\{\dot{q}_2\} + [K_{12}]\{q_2\} = \left\{F_{u1}(t)\right\}, \end{aligned} \tag{15}$$

$$\begin{aligned} &[M_{22}]\{\ddot{q}_2\} + [C_{22}]\{\dot{q}_2\} + [K_{22}]\{q_2\} + [M_{21}]\{\ddot{q}_1\} \\ &\quad + [C_{21}]\{\dot{q}_1\} + [K_{21}]\{q_1\} \\ &= \left\{F_{u2}(t)\right\} + \left\{F_{s2}\left(\{q_2\},\{\dot{q}_2\}\right)\right\}. \end{aligned} \tag{16}$$

Newmark-β method is an immediate integration in common use. According to its fundamental assumption, $\{\ddot{q}\}^{t+\Delta t}$ and $\{\dot{q}\}^{t+\Delta t}$ at time $t+\Delta t$ can be described as follows:

$$\begin{aligned} \{\ddot{q}\}^{t+\Delta t} &= \frac{1}{\alpha\Delta t^2}\{q\}^{t+\Delta t} - \frac{1}{\alpha\Delta t^2}\{q\}^t \\ &\quad - \frac{1}{\alpha\Delta t}\{\dot{q}\}^t - \left(\frac{1}{2\alpha}-1\right)\{\ddot{q}\}^t, \end{aligned} \tag{17}$$

$$\begin{aligned} \{\dot{q}\}^{t+\Delta t} &= \frac{\delta}{\alpha\Delta t}\{q\}^{t+\Delta t} - \frac{\delta}{\alpha\Delta t}\{q\}^t + \left(1-\frac{\delta}{\alpha}\right)\{\dot{q}\}^t \\ &\quad + \left(1-\frac{\delta}{2\alpha}\right)\Delta t\{\ddot{q}\}^t, \end{aligned} \tag{18}$$

where α and δ are two parameters used in the Newmark-β method.

Introducing (17) and (18) into (15), and defining

$$\begin{aligned} [\bar{K}_{11}] &= [K_{11}] + \frac{1}{\alpha\Delta t^2}[M_{11}] + \frac{\delta}{\alpha\Delta t}[C_{11}], \\ [\bar{K}_{12}] &= [K_{12}] + \frac{1}{\alpha\Delta t^2}[M_{12}] + \frac{\delta}{\alpha\Delta t}[C_{12}], \\ [\bar{F}_{u1}] &= [F_{u1}]^{t+\Delta t} - [M_{11}]\{\ddot{q}_1\} - [C_{11}]\{\dot{q}_1\} \\ &\quad - [M_{12}]\{\ddot{q}_2\} - [C_{12}]\{\dot{q}_2\}, \end{aligned} \tag{19}$$

we have

$$\{q_1\}^{t+\Delta t} = [\bar{K}_{11}]^{-1}\{\bar{F}_{u1}\} - [\bar{K}_{11}]^{-1}[\bar{K}_{12}]\{q_2\}^{t+\Delta t}. \tag{20}$$

We next introduce (17), (18), and (20) into (16), and define

$$\begin{aligned} [\bar{K}_{21}] &= [K_{21}] + \frac{1}{\alpha\Delta t^2}[M_{21}] + \frac{\delta}{\alpha\Delta t}[C_{21}], \\ [\bar{K}_{22}] &= [K_{22}] + \frac{1}{\alpha\Delta t^2}[M_{22}] + \frac{\delta}{\alpha\Delta t}[C_{22}] \\ &\quad - [\bar{K}_{21}][\bar{K}_{11}]^{-1}[\bar{K}_{12}], \end{aligned} \tag{21}$$

$$[\bar{F}_{u2}] = [F_{u2}]^{t+\Delta t} - [M_{21}]\{\ddot{q}_1\} - [C_{21}]\{\dot{q}_1\} - [M_{22}]\{\ddot{q}_2\} - [C_{22}]\{\dot{q}_2\} - [\bar{K}_{21}][\bar{K}_{11}]^{-1}[\bar{F}_{u1}].$$

Then, we have

$$[\bar{K}_{22}]\{q_2\}^{t+\Delta t} = \{\bar{F}_{u2}\} + \{F_{s2}\} \tag{22}$$

which are low-order nonlinear equations. Using the Newton–Raphson approach, (22) can be solved by iteration and $\{q_2\}^{t+\Delta t}$ can be obtained. Then, all that is needed is to solve the linear algebraic equations, (20), and determine $\{q_1\}^{t+\Delta t}$. It can be found that the computational efforts using the proposed method are greatly reduced as a result of the iterative computation operated with low-order equations instead of high-order system equations. This approach, called the partitioned direct integration method (PDIM), is common and efficient. It can be employed to calculate the transient responses of complex rotor systems that endure nonlinear forces at limited locations.

Combined with the presented PDIM, the shooting method can be utilized to analyze the synchronous solution of the nonlinear turbopump rotor system effectively. Therefore, the nonlinear stability analysis of the parametrically excited system is performed with the aid of the Floquet theory [25]. With the gained Floquet multipliers $|\lambda_i| < 1, (i = 1, 2, \ldots, 44)$, the synchronous solution of the system is stable in the Lyapunov sense. If at least one Floquet multiplier exists with an absolute value higher than unity, the response will grow as time increases and the solution will be unstable. If the maximal absolute value of λ_i equals unity, the solution will be critically stable and the boundary between the stable and unstable regions is determined.

4 Nonlinear rotordynamic analysis of the rotor system with flexible support

Two designs have been performed in the development efforts of the liquid fuel turbopump, as shown in Fig. 1.

Table 1 Specifications of seal used in the liquid fuel turbopump

c mm	R mm	L mm	n	b	τ_0	Re_a	ν $\mathrm{N\,s\,m^{-2}}$
0.15	45.3	21.0	2.5	0.5	0.49	300,000	1.093×10^{-6}

The first design is that the turbine bearing, like the pump bearing, is fixed on a bearing block directly. The bearing stiffness is modeled as $k = k_{uu} = k_{vv} = 6.5 \times 10^7$ N/m, $k_{uv} = k_{vu} = 0$. In the second design, the turbine bearing is carried by a flexible support as the pump bearing is still fixed on the bearing block. Because of the support modification at the turbine end from rigid to flexible, the support stiffness is decreased to $k = k_{uu} = k_{vv} = 1.5 \times 10^7$ N/m. Note that the parameter k is designated as the support stiffness at turbine end in the following.

When $k = 6.5 \times 10^7$ N/m, the measured values of system external damping are {47.64, 60.05, 67.18, 68.20} N s/m corresponding to the impeller, the gear, and two bellows seals, which are located at nodes 4, 6, 8, and 9, respectively. The coefficient of internal viscous damping measures $\eta_v = 1700$ N s/m^2, and the hysteretic factor measures $\eta_h = 0.00015$. The experimental data indicated that the external damping at $k = 1.5 \times 10^7$ N/m is 2∼3 times and the internal damping is about 26% of that at $k = 6.5 \times 10^7$ N/m. The specifications of the seal are given in Table 1.

The mass eccentricity of the pump end could rise significantly due to the different cryogenic shrinkages of the shaft and impeller material. In the analysis, it is assumed that the mass eccentricity of the pump end disk is 0.01 mm. The different destabilizing factors, internal damping and/or seal, are taken into account to investigate their effects on the dynamic characteristics and stability of the system. The first and second forward critical speeds are denoted by ω_{c1} and ω_{c2}, respectively. Below a given operating speed, "the onset speed of instability," denoted by ω_s, the rotor's motion is stable and synchronous. Above this speed, there is a subsynchronous frequency component to the rotor's motion, denoted by Ω.

The numerical results and test data of two designs, $k = 6.5 \times 10^7$ N/m and $k = 1.5 \times 10^7$ N/m, are listed in Table 2. It can be found that the predicted results match the experimental data quite well, and the effects of the flexible support stiffness on the critical speeds and stability of the turbopump rotor system are remarkable. Although the effects of the seal on the critical speeds are insignificant, the effects of the seal on the onset speed of instability are significant. Moreover, the effects of seal nonlinearities on system stability at $k = 1.5 \times 10^7$ N/m are greater than those at $k = 6.5 \times 10^7$ N/m.

When $k = 6.5 \times 10^7$ N/m, the seal's effects increase the onset speed of instability from $\omega_s = 3666.1$ rad/s

Table 2 Numerical results and test data of two designs

k $10^7 \times$ N/m	Influence factors	ω_{c1} rad s^{-1}	ω_{c2} rad s^{-1}	ω_s rad s^{-1}	Ω rad s^{-1}
6.5	Internal damping	2814.2	6185.3	3666.1	2916∼3061
	Seal and internal damping	2815.5	6185.0	3883.0	2932∼3075
	Test data	2820	–	> 3800	2820∼3330
1.5	Internal damping	1542.6	6165.8	7727.4	1870∼1907
	Seal and internal damping	1553.0	6163.7	7073.4	1855∼1890
	Test data	1570	–	6910	–

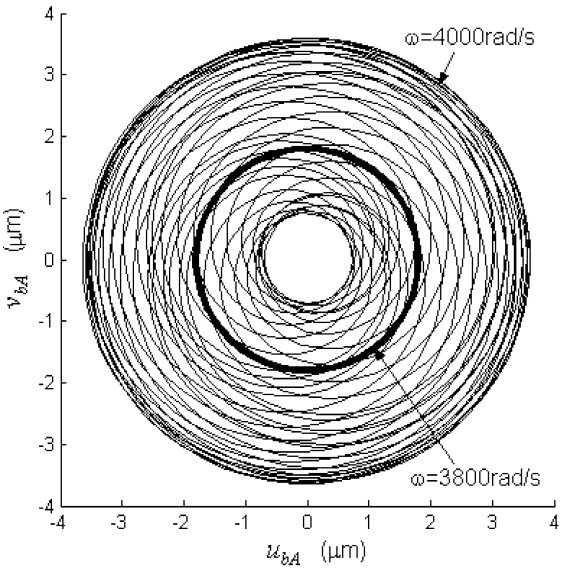

(a) Orbit at pump end support

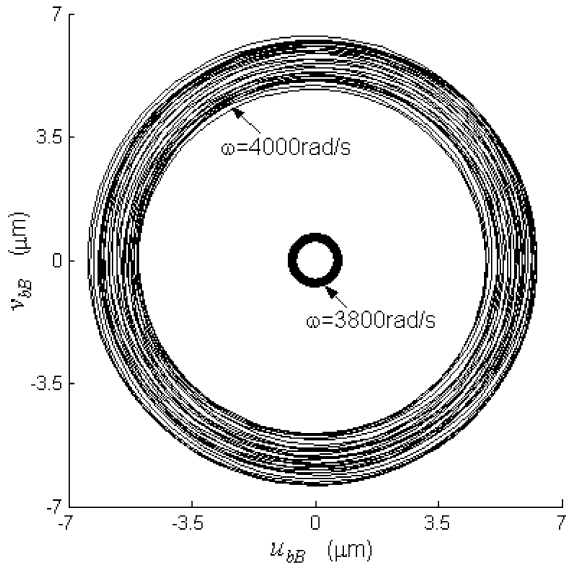

(b) Orbit at turbine end support

Fig. 2 Orbit comparisons for stable and unstable system at $k = 6.5 \times 10^7$ N/m

Table 3 First three critical speeds versus flexible support stiffness

k $10^7 \times$ N/m	ω_{c1} rad s^{-1}	ω_{c2} rad s^{-1}	ω_{c3} rad s^{-1}
0.5	928.05	6159.00	12765.14
1.0	1289.53	6161.38	12813.21
1.5	1553.01	6163.71	12859.25
2.0	1764.62	6166.00	12903.35
2.5	1942.63	6168.26	12945.58
3.0	2096.60	6170.47	12986.02
3.5	2232.28	6172.65	13024.75
4.0	2353.48	6174.79	13061.85
4.5	2462.88	6176.89	13097.39
5.0	2562.44	6178.96	13131.44
5.5	2653.65	6180.99	13164.07
6.0	2737.69	6182.98	13195.34
6.5	2815.49	6184.95	13225.33
7.0	2887.80	6186.88	13254.08
7.5	2955.27	6188.77	13281.67

to $\omega_s = 3883.0$ rad/s, and also somewhat the subsynchronous frequency component. When the seal nonlinearities are taken into account, the predicted results are much more close to the test data. Figure 2 plots the shaft center orbits at the pump and turbine end supports for comparison between system stable motion at $\omega = 3800$ rad/s and unstable motion at $\omega = 4000$ rad/s. It is shown that the amplitude at both supports rises dramatically when the system motion is unstable above ω_s. When $\omega = 4000$ rad/s $> \omega_s$, the amplitude spectrum and Poincaré maps of the system unstable responses at both supports are illustrated in Fig. 3 and Fig. 4, respectively. It shows that the subsynchronous frequency component, Ω, occurs in the amplitude spectrum for both supports' responses. The quasi-periodic motions emerge at both supports through sec-

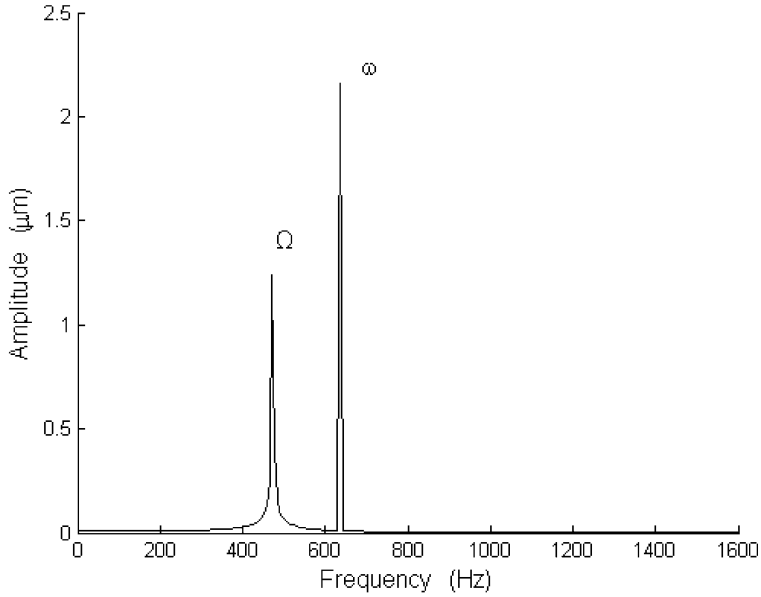

(a) Amplitude spectrum at pump end support

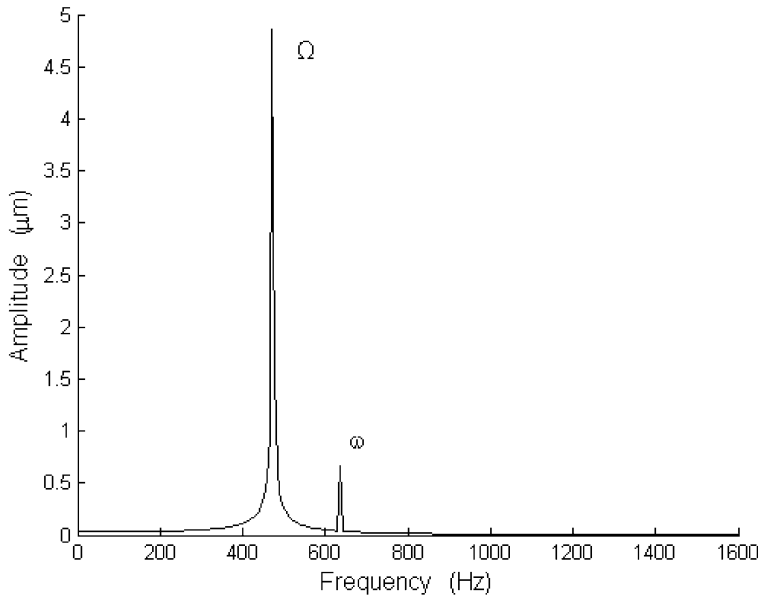

(b) Amplitude spectrum at turbine end support

Fig. 3 Amplitude spectrum comparisons for two end supports at $\omega = 4000$ rad/s and $k = 6.5 \times 10^7$ N/m

ondary Hopf bifurcation, as shown in Figs. 2 and 4. The damaging subsynchronous whirling motion at the turbine end support is more significant than that at the pump end support when the rotational speed of the rotor system is above ω_s.

When the flexible support is modified at the turbine end and $k = 1.5 \times 10^7$ N/m, as shown in Table 3, the first critical speed, ω_{c1}, decreases considerably and the onset speed of instability, ω_s, increases significantly compared with that when $k = 6.5 \times 10^7$ N/m. The predicted stability results are in good agreement with test data when the seal nonlinearities are considered, which indicates that the seals play an essential role in system stability in this design. Note that ω_s decreases remarkably due to the effect of the seal at $k = 1.5 \times 10^7$ N/m, but in contrast, it increases at $k = 6.5 \times 10^7$ N/m. Figure 5 provides the shaft center orbits at the pump and turbine end supports. It can

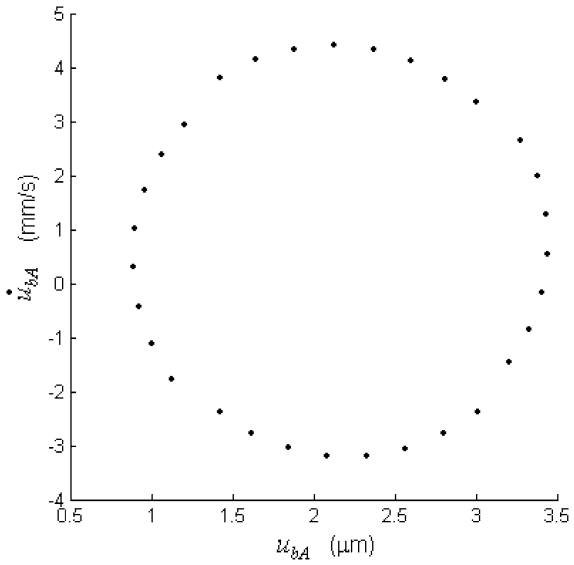

(a) Poincarè map at pump end support

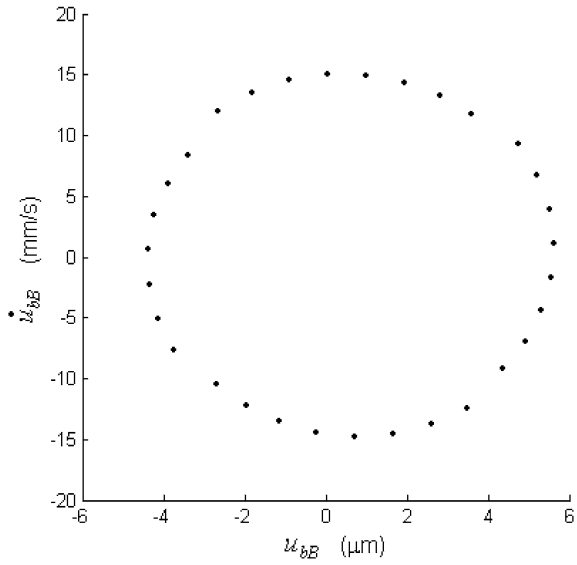

(b) Poincarè map at turbine end support

Fig. 4 Poincaré map comparisons for two end supports at $\omega = 4000$ rad/s and $k = 6.5 \times 10^7$ N/m

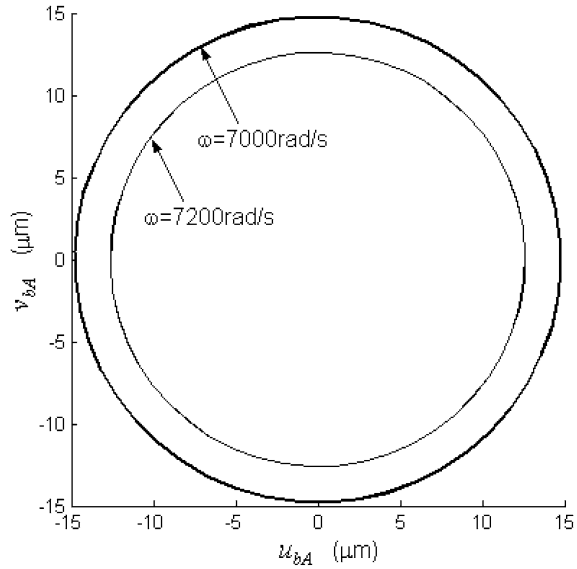

(a) Orbit at pump end support

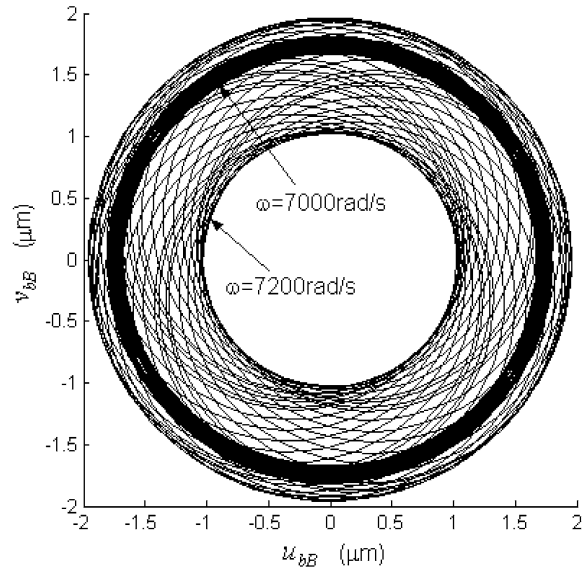

(b) Orbit at turbine end support

Fig. 5 Orbit comparisons for stable and unstable system at $k = 1.5 \times 10^7$ N/m

be found that the orbit at the pump end support is a periodic motion and the amplitude is reduced as the rotational speed increases from $\omega = 7000$ rad/s $< \omega_s$ to $\omega = 7200$ rad/s $> \omega_s$. However, the subsynchronous motion occurs at the turbine end support when $\omega > \omega_s$. From the amplitude spectrum at $\omega = 7200$ rad/s, as shown in Fig. 6, it is shown that the subsynchronous frequency component, Ω, rises only from the vibration at the turbine end support. Poincaré maps, as depicted in Fig. 7, indicate that the motion at the pump end support keeps a periodic response, and the periodic response at the turbine end support loses stability through a secondary Hopf bifurcation to a quasi-periodic motion when $\omega = 7200$ rad/s $> \omega_s$. In contrast with the subsynchronous whirling motion at both supports at $k = 6.5 \times 10^7$ N/m when $\omega > \omega_s$ (shown in Figs. 2–4), it can be found that the effects of flexible support stiffness on the rotordynamic characteristics

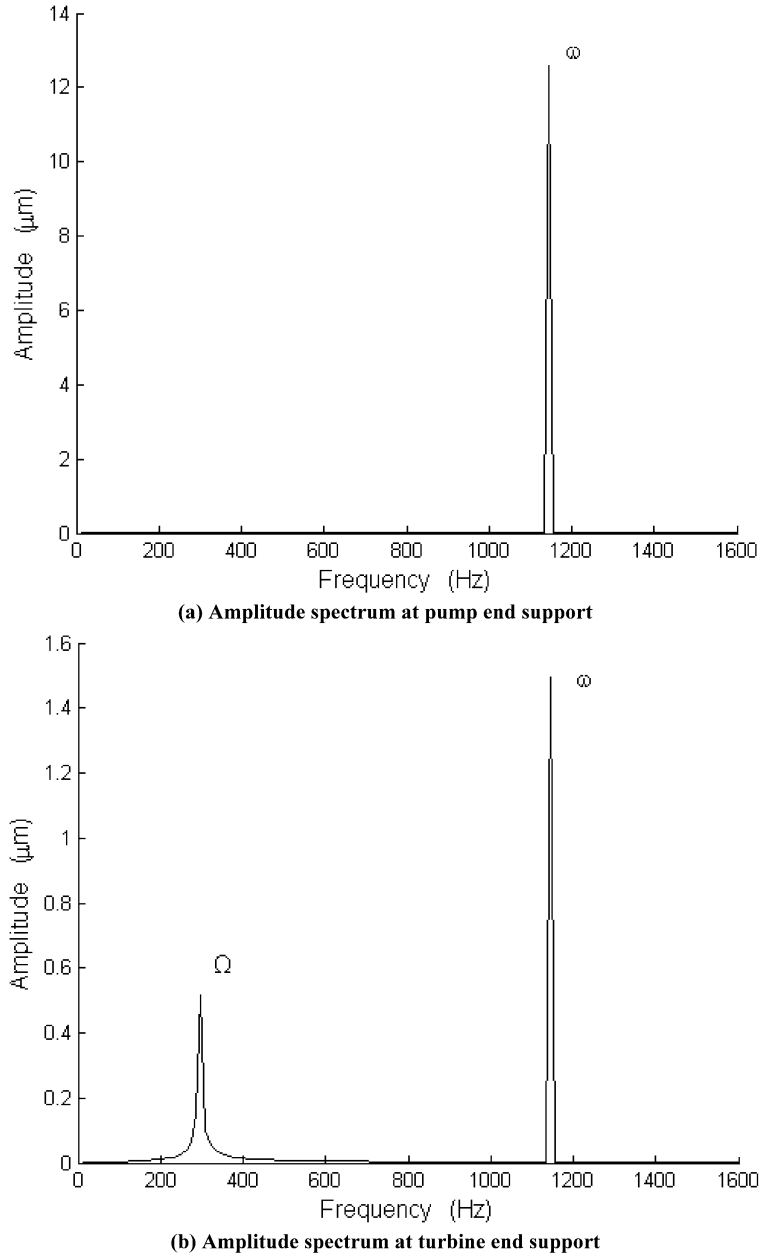

(a) Amplitude spectrum at pump end support

(b) Amplitude spectrum at turbine end support

Fig. 6 Amplitude spectrum comparisons for two end supports at $\omega = 7200$ rad/s and $k = 1.5 \times 10^7$ N/m

and stability of the turbopump rotor system are significant and complex.

Using the PDIM, the imbalance responses of the turbopump rotor system are calculated efficiently to obtain the system critical speed where the system external and internal damping at different k are determined according to the linear interpolation of the test data. Table 3 lists the first three critical speeds versus the flexible support stiffness k of the turbopump rotor system. For clarity, the relative variation of the critical speed on k, defined as the critical speed at arbitrary k minus that at minimum k, is described in Fig. 8 when the origin is defined at the critical speed at $k = 0.5 \times 10^7$ N/m. It can be seen that the variation of the first critical speed rises as a nonlinear function of k significantly. But the second critical speed varies slightly as k increases. The second and third critical speeds versus k approximate a linear varia-

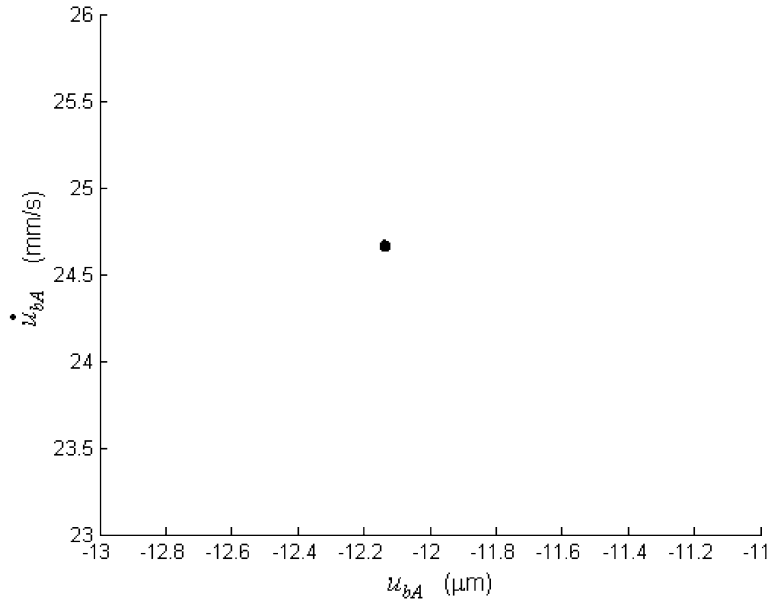

(a) Poincarè map at pump end support

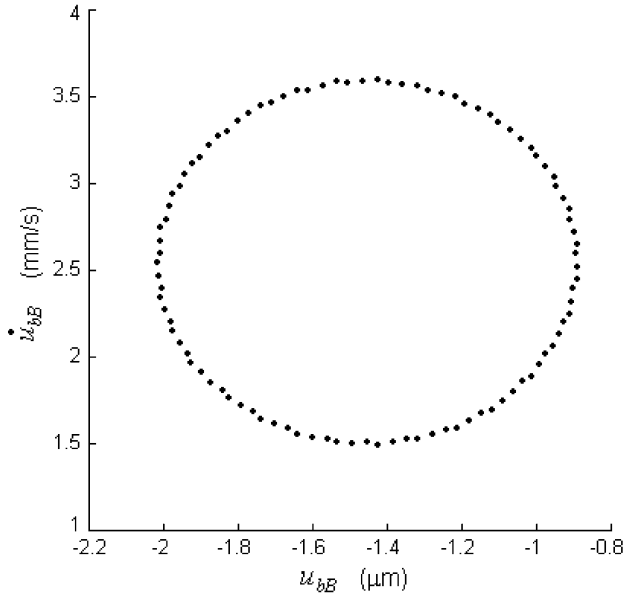

(b) Poincarè map at turbine end support

Fig. 7 Poincaré map comparisons for two end supports at $\omega = 7200$ rad/s and $k = 1.5 \times 10^7$ N/m

tion, which implies that the seal nonlinearities are directly bound up with the first critical speed of the rotor system. Figures 9 and 10 plot the first three mode shapes at $k = 6.5 \times 10^7$ N/m and $k = 1.5 \times 10^7$ N/m, respectively. It is shown that the first mode shape at $k = 6.5 \times 10^7$ N/m is in the vicinity of that at $k = 1.5 \times 10^7$ N/m, except for the slight variance of the shape curvature. However, the second and third mode shapes at $k = 6.5 \times 10^7$ N/m are dramatically different from those at $k = 1.5 \times 10^7$ N/m. The obvious differences of mode characteristics, critical speeds, and mode shapes can induce a considerable modification of system dynamic responses. This indicates that the flexible support stiffness has a notable impact on the dynamic characteristics of the turbopump rotor system when $\omega > \omega_{c2}$. The differences of system dynamic responses on k, as shown in Fig. 2 and Fig. 5, are due in part to the modification of mode shape.

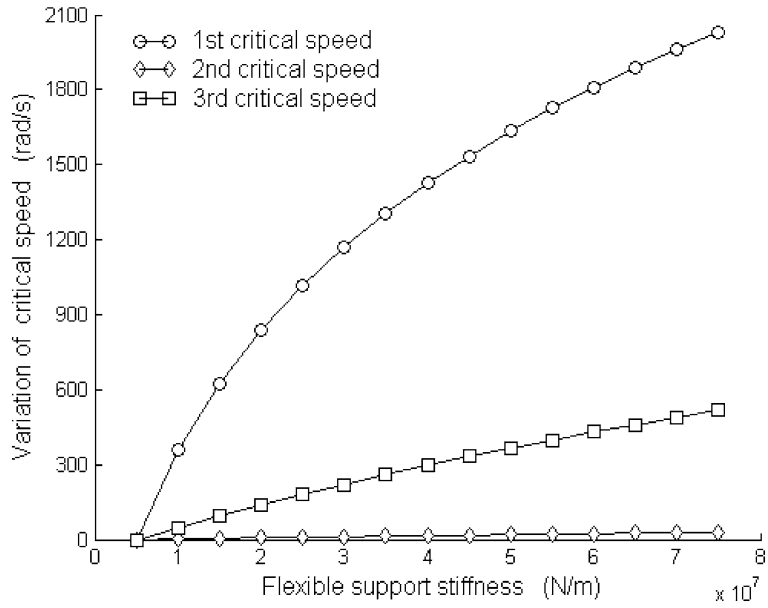

Fig. 8 Relative variation of system critical speed on flexible support stiffness

Note that the first mode shape plays a key role in the vibratory response of the rotor system. It is found that the vibration at the turbine end support is more severe than the vibration at the pump end support in the first mode shape at $k = 6.5 \times 10^7$ N/m, as shown in Fig. 9. The damaging subsynchronous motion at the turbine end support is more significant than that at the pump end support, when the remarkable vibration can induce the subsynchronous motion on account of the internal damping, as shown in (4) and (5). As shown in Fig. 10, it can be seen that the vibration at the turbine end support in the first mode shape is far more significant than the vibration at the pump end support; that is, the turbine end vibration in the first mode shape at $k = 1.5 \times 10^7$ N/m is more significant than that at $k = 6.5 \times 10^7$ N/m. It causes the subsynchronous motion to occur at the turbine end support first when $\omega = \omega_s$. As the rotational speed increases, the subsynchronous whirling motion propagates from turbine end to pump end.

Figure 11 depicts the effect of flexible support stiffness on the stability of the turbopump rotor system. It can be found that the onset speed of instability rises initially and then reduces as k increases, since the mode shapes, especially the second mode shape, and system damping determined according to the test data change as k increases. It is shown that the effect of the seal on the system stability varies greatly according to the value of k. It is well known that the single seal hydrodynamic forces can induce a subsyn-

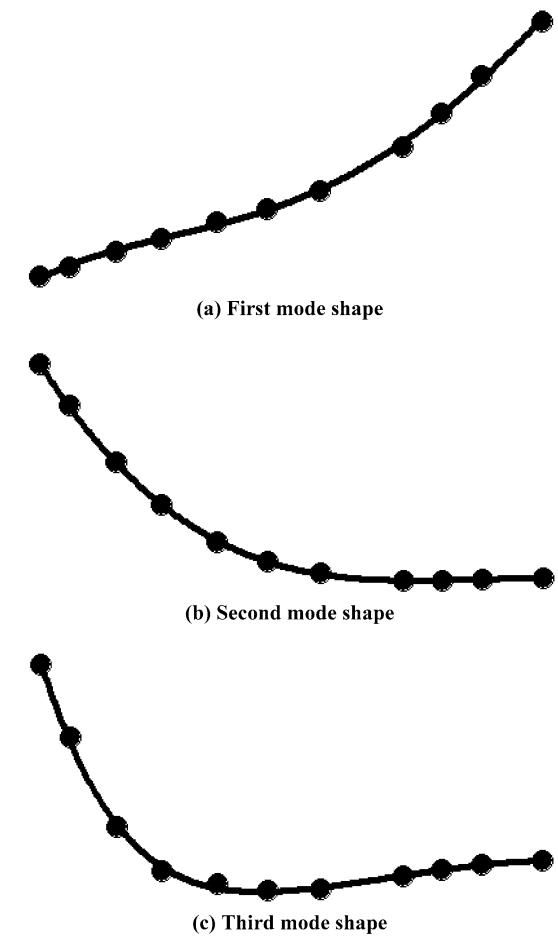

Fig. 9 First three mode shapes at $k = 6.5 \times 10^7$ N/m

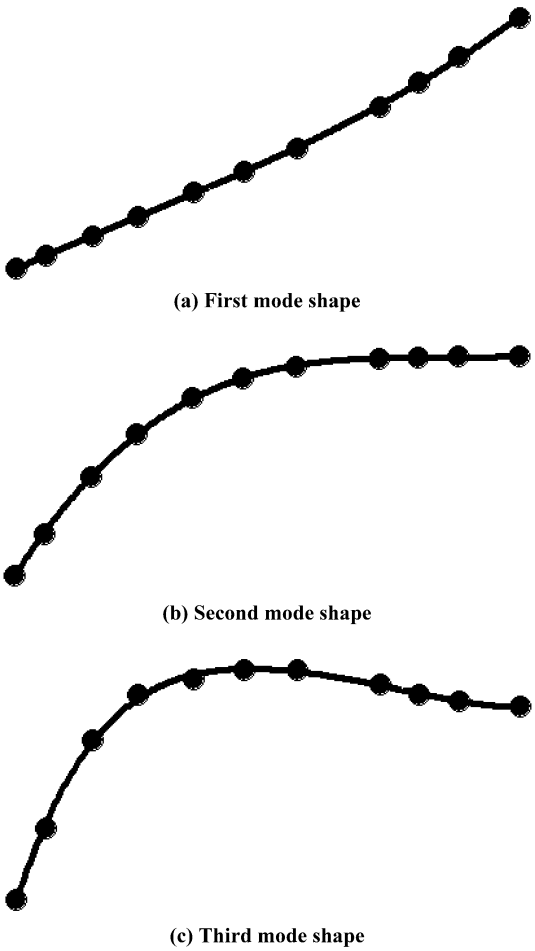

Fig. 10 First three mode shapes at $k = 1.5 \times 10^7$ N/m

chronous whirling motion when the rotational speed is about twice critical speed. With regard to the turbopump rotor system including two key destabilizing factors, seal and internal rotor damping, the seal forces could have different effects on the system stability as the onset speed of instability is below or above twice critical speed. As shown in Fig. 11, the onset speed of instability decreases as $k < 4.0 \times 10^7$ N/m and increases as $k > 4.0 \times 10^7$ N/m. The effect of the seal on the system stability is insignificant as k is near 4.0×10^7 N/m.

Since the seals of the turbopump influence the system stability markedly, one should consider the effect of the seal parameters on the system stability. The seal length L and radius R are two important parameters in a turbopump design. As shown in Fig. 12(a) and Fig. 12(b), the effects of seal radius variation on the onset speed of instability as a function of seal length are illustrated at $k = 6.5 \times 10^7$ N/m and $k = 1.5 \times 10^7$ N/m, respectively. One must denote that the ratio of seal clearance to radius is constant when the seal radius varies from $R = 30$ mm to $R = 60$ mm. From Fig. 12, it can be seen that the onset speed of instability increases as the seal length and radius increase at $k = 6.5 \times 10^7$ N/m. However, the onset speed of instability decreases as the seal length and radius rise at $k = 1.5 \times 10^7$ N/m because of the changes of seal effects and system mode shapes on k. Otherwise, the effect of seal length on the system stability is more significant than that of seal radius.

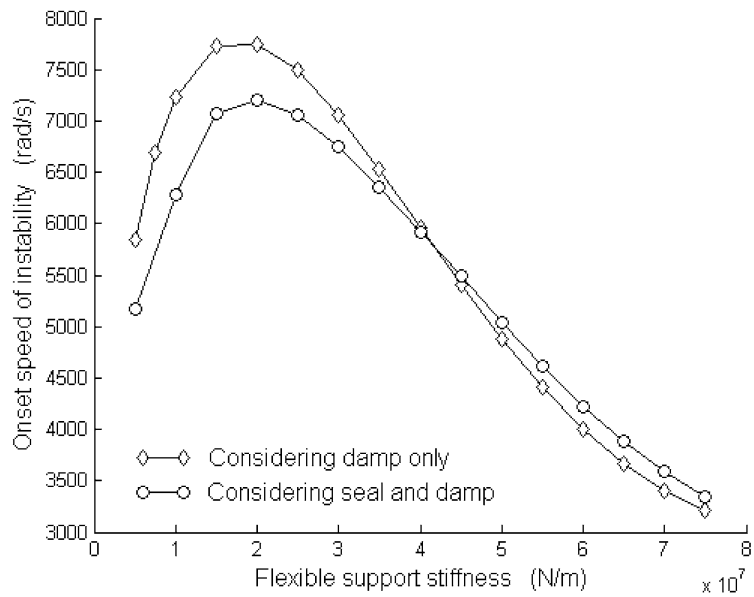

Fig. 11 Onset speed of instability versus flexible support stiffness

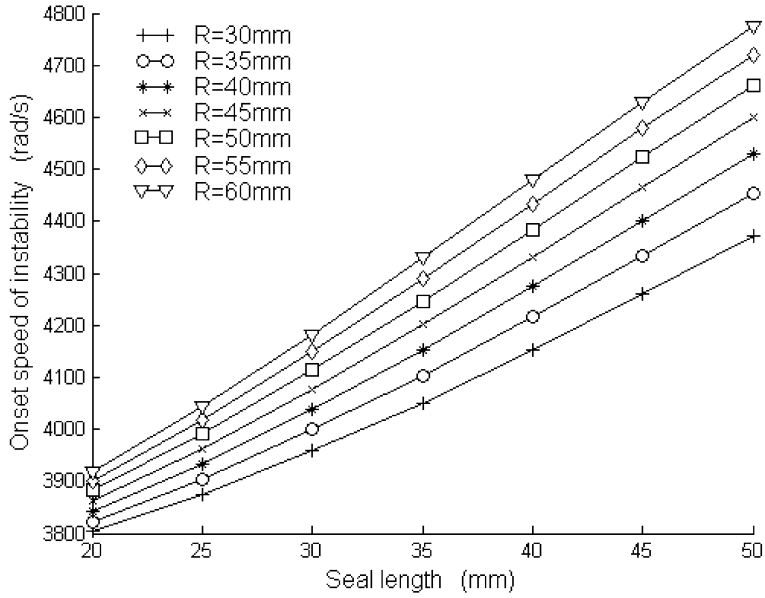

(a) Onset speed of instability versus seal length at k=6.5×10^{7}N/m

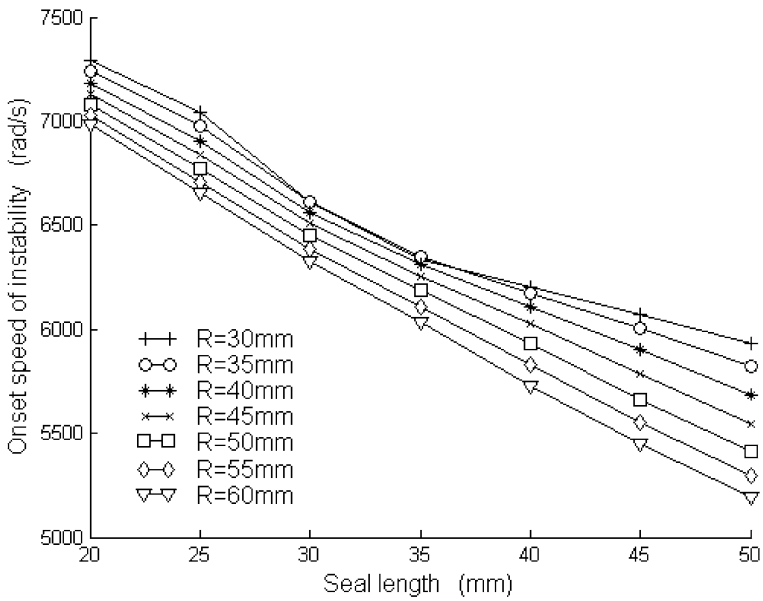

(b) Onset speed of instability versus seal length at k=1.5×10^{7}N/m

Fig. 12 Effect of seal length and radius on onset speed of instability

5 Conclusions

Using the partitioned direct integration method (PDIM), the effects of flexible support stiffness on the nonlinear rotordynamic characteristics and stability of a liquid fuel turbopump rotor system are investigated with a dynamic modeling that includes the effects of internal damping and seal nonlinearities. From the results presented in this paper, the following conclusions can be drawn.

1. The predicated results are in good agreement with test data and indicate that the effects of flexible support stiffness k on system characteristics and stability are significant.
2. When $k = 6.5 \times 10^7$ N/m, subsynchronous whirling motions emerge at both supports when the rota-

tional speed of the rotor system ω is above the onset speed of instability ω_s. When a flexible support is employed at the turbine end and the support stiffness is decreased to $k = 1.5 \times 10^7$ N/m, the motion at the pump end support keeps a periodic response, and the periodic response at the turbine end support loses stability through a secondary Hopf bifurcation to a quasi-periodic motion when $\omega > \omega_s$.

3. The first critical speed of the turbopump rotor system rises markedly as a nonlinear function of k. But the second critical speed varies slightly as k increases, and the second and third critical speeds versus k approximate a linear variation. This implies that the seal nonlinearities are directly bound up with the first critical speed of the rotor system. The mode shapes except for the first mode shape have significant changes as k varies.
4. The onset speed of instability of the rotor system rises initially and then reduces as k increases. The effects of seal nonlinearities at low stiffness of the flexible support are greater than those at high stiffness. The onset speed of instability decreases when the stiffness is low and increases when the stiffness is high because of the seal effects on the system stability.
5. The onset speed of instability decreases as the seal length and radius rise at low stiffness. However, the onset speed of instability increases as the seal length and radius increase at high stiffness. The effect of seal length on the system stability is more significant than that of the seal radius.

Acknowledgements The authors would like to acknowledge the support of the National Natural Science Foundation of China (10902080, 11002106), the Research Fund for the Doctoral Program of Higher Education (20090201120040), and the Fundamental Research Funds for the Central Universities.

Appendix

The coefficients K_0, D_0 and m_f can be expressed as

$$K_0 = \mu_3\mu_0, \qquad D_0 = \mu_1\mu_3 T, \qquad m_f = \mu_2\mu_3 T^2, \tag{23}$$

where

$$\mu_0 = \frac{2\sigma^2}{1+z+2\sigma}E(1-m_0), \tag{24}$$

$$\mu_1 = \frac{2\sigma^2}{1+z+2\sigma}\left[\frac{E}{\sigma} + \frac{B}{2}\left(\frac{1}{6}+E\right)\right], \tag{25}$$

$$\mu_2 = \frac{\sigma(1/6+E)}{1+z+2\sigma}, \qquad \mu_3 = \frac{\pi R\Delta P}{\lambda}, \qquad T = \frac{L}{v_a}, \tag{26}$$

where

$$\lambda = n_0 \mathrm{Re}_a^{m_0}\left[1+\left(\frac{\mathrm{Re}_v}{\mathrm{Re}_a}\right)^2\right]^{\frac{1+m_0}{2}}, \qquad \sigma = \frac{\lambda L}{c}, \tag{27}$$

$$E = \frac{1+z}{1+z+2\sigma}, \qquad B = 2 - \frac{\left(\frac{\mathrm{Re}_v}{\mathrm{Re}_a}\right)^2 - m_0}{\left(\frac{\mathrm{Re}_v}{\mathrm{Re}_a}\right)^2 + 1}. \tag{28}$$

The axial and radial Reynolds numbers, Re_v and Re_a, are defined by

$$\mathrm{Re}_v = \frac{Rc_d\omega}{\nu}, \qquad \mathrm{Re}_a = \frac{2v_a c}{\nu}. \tag{29}$$

In these equations, ΔP, z, v_a and ν are the pressure margin of the seal, inlet loss coefficient, axial fluid speed, and fluid dynamic viscous coefficient, respectively. m_0 and n_0 are experiential coefficients, determined by experiments and the material structure of the seal.

References

1. Ek, M.C.: Solution of the subsynchronous whirl problem in the high pressure hydrogen turbomachinery of the space shuttle main engine. In: AIAA/SAE 14th Joint Propulsion Conference, Las Vegas, NV (1978)
2. Childs, D.W.: The space shuttle main engine high-pressure fuel turbopump rotordynamic instability problem. ASME J. Eng. Power **100**(1), 48–57 (1978)
3. Childs, D.W.: Turbomachinery Rotordynamics: Phenomena, Modeling, and Analysis. Wiley, New York (1993)
4. Ying, G.L.: Vibration analysis of LH_2 turbopump test. Missiles Space Veh. **5**, 40–46 (1995)
5. Okayasu, A., Ohta, T., Azuma, T.: Vibration problem in the LE-7 LH2 turbopump. In: SAE, ASME, and ASEE, 26th Joint Propulsion Conference, Orlando, FL (1990)
6. Chen, L.: Stability analysis of rotor-bearing system using finite element method. Dissertation, the Eleventh Institute of China Ministry of Aerospace Industry (1986)
7. Zhang, X.L.: Research on the critical speed of liquid hydrogen turbopump rotor system and its subsynchronous motion. Dissertation, Northwestern Polytechnical University (2000)
8. Black, H.F.: Effects of hydraulic forces in annular pressure seals on the vibration of centrifugal pump rotors. J. Mech. Eng. Sci. **11**(4), 206–213 (1969)

9. Muszynska, A.: A whirl and whip rotor/bearing stability problems. J. Sound Vib. **110**(3), 443–462 (1986)
10. Muszynska, A., Bently, D.E.: Frequency-swept rotating input perturbation techniques and identification of the fluid force models in rotor/bearing/seal systems and fluid handling machines. J. Sound Vib. **143**(1), 103–124 (1990)
11. Ding, Q., Cooper, J.E., Leung, A.Y.T.: Hope bifurcation analysis of a rotor/seal system. J. Sound Vib. **252**(5), 817–833 (2002)
12. Li, S.T., Xu, Q.Y., Zhang, X.L.: Nonlinear stability behaviors of a rotor-labyrinth seal system. Nonlinear Dyn. **47**, 321–329 (2007)
13. Bai, C.Q., Xu, Q.Y., Zhang, X.L.: Nonlinear dynamic stability of liquid hydrogen turbopump rotor-seal system used in rocket engine. J. Xi'an Jiaotong Univ. **39**(9), 1016–1020 (2005)
14. Nicholas, J.C., Whalen, J.K., Franklin, S.D.: Improving critical speed calculations using flexible bearing support FRF compliance data. In: Proceedings of the Turbomachinery Symposium, Texas A&M University, College Station, TX, pp. 69–78 (1986)
15. Guo, Z.L., Kirk, R.G.: Instability boundary for rotor-hydrodynamic bearing systems, Part 2: Rotor with external flexible damped support. ASME J. Vib. Acoust. **125**(4), 423–426 (2003)
16. Seong, M.J., Hyun, D.K., Suk, H.Y., Jinhan, K.: Rotordynamic analysis of a turbopump with the casing structural flexibility. J. Propuls. Power **24**(3), 433–436 (2008)
17. Qin, W.Y., Zhang, J.F., Ren, X.M.: Response and bifurcation of rotor with squeeze film damper on elastic support. Chaos Solitons Fractals **39**(1), 188–195 (2009)
18. Chang-Jian, C., Chen, C.: Nonlinear analysis of a rub-impact rotor supported by turbulent couple stress fluid film journal bearings under quadratic damping. Nonlinear Dyn. **56**(3), 297–314 (2009)
19. Chang-Jian, C., Chen, C.: Chaotic response and bifurcation analysis of a flexible rotor supported by porous and non-porous bearings with nonlinear suspension. Nonlinear Anal., Real World Appl. **10**(2), 1114–1138 (2009)
20. Nelson, H.D.: A finite rotating shaft element using Timoshenko beam theory. ASME J. Mech. Des. **102**, 793–803 (1980)
21. Gunter, E.J.: The influence of internal friction on the stability of high speed rotors. ASME J. Eng. Ind. **89**, 683–692 (1967)
22. Hashish, E., Sankar, T.S.: Finite element and modal analyses of rotor-bearing systems under stochastic loading conditions. ASME J. Vib. Acous. Stress Reliab. Des. **106**, 80–89 (1984)
23. Childs, D.W.: Dynamic analysis of turbulent annular seals based on Hirs lubrication equation. ASME J. Lubr. Technol. **105**(3), 429–436 (1983)
24. Li, L., Xu, Q.Y., Zhen, T.S.: Partitioned direct integration methods for transient response of nonlinear rotor-bearing systems. J. Vib. Eng. **9**(1), 64–68 (1996)
25. Zhou, J.Q., Zhu, Y.Y.: Nonlinear Vibrations. Xi'an Jioatong University Press, Xi'an (1998)